J. Fluid Mech. (1997), *vol.* 352, *pp.* 1–25. Printed in the United Kingdom

© 1997 Cambridge University Press

Numerical study of inviscid shock interactions on double-wedge geometries

By JOSEPH OLEJNICZAK, MICHAEL J. WRIGHT AND GRAHAM V. CANDLER

Department of Aerospace Engineering and Mechanics, Army High Performance Computing Research Center, University of Minnesota, 110 Union Street SE, Minneapolis, MN 55455, USA
e-mail: candler@aem.umn.edu

(Received 19 November and in revised form 3 July 1997)

Computational fluid dynamics has been used to study inviscid shock interactions on double-wedge geometries with the purpose of understanding the fundamental gas dynamics of these interactions. The parameter space of the interactions has been explored and the different types of interactions that occur have been identified. Although the interactions are produced by a different geometry, all but one of them may be identified as an Edney Type I, IV, V, or VI interaction. The previously unidentified interaction occurs because of the geometrical constraints imposed by the double wedge. The physical mechanisms for transition have been studied, and the transition criteria have been identified. An important result is that there are two different regimes of the parameter space in which the state of the flow downstream of the interaction point is fundamentally different. At high Mach numbers this flow is characterized by an underexpanded jet which impinges on the wedge and produces large-amplitude surface pressure variations. At low Mach numbers, the jet becomes a shear layer which no longer impinges on the wedge surface.

1. Introduction

Edney (1968) studied the interaction of an oblique shock wave and a bow shock wave on a cylinder. He used shock polars to classify the interactions that he observed in his experiments. Edney's classification scheme is now widely used to categorize shock interactions. In this paper, we use computational fluid dynamics to study shock interactions generated by double-wedge geometries. We show that, with one exception, Edney's classification scheme may be applied to these flows.

Edney's work was motivated by the practical problem of understanding unexplained transient heating loads during the insertion of models into supersonic wind tunnels. This work led to the realization that shock interactions can cause anomalously high heating and pressure loads on supersonic and hypersonic vehicles. A dramatic example of this effect was the airframe damage to the X-15 caused by a shock interaction. During a flight in which a ram-jet test model was attached to the ventral fin of the X-15, an unforeseen shock interaction produced high heating loads which burned through the fin and resulted in the loss of the ram-jet. There was also concern about the interaction between fuselage-generated and wing-generated shocks on preliminary Space Shuttle configurations. Later, there was renewed interest in shock interactions when it was discovered that extremely high heating loads were possible at the engine inlet cowl on the proposed National Aerospace Plane due to shock interaction heating.

https://doi.org/10.1017/S0022112097007131 Published online by Cambridge University Press

Because of these technological issues, a large number of papers have been published on this topic.

Recently, we used shock interactions on double-wedge and double-cone geometries to study chemical kinetics models used in reacting hypersonic flows (Olejniczak *et al.* 1996; Olejniczak & Candler 1996). Our experimental results and numerical simulations of these flows raised many questions. In particular, we could not understand the source of large-amplitude steady-state variations in surface pressure and heat transfer rate. Also, surprisingly small changes in the geometry led to large changes in the overall flow structure. These flows are complicated by the fact that finite-rate chemical reactions are coupled to the fluid motion and that viscous effects play a large role. The additional length scales introduced into the flow by real gas and viscous effects make the analysis very difficult, or even impossible. There is a need for a fundamental study that will aid in the analysis of future experiments and calculations that include these effects. Therefore, in the current paper we study inviscid, perfect gas shock interactions on double-wedge geometries, with the purpose of better understanding the gas dynamics of the resulting shock interactions. We use computational fluid dynamics to study these flows, so that we may systematically explore the effects of the governing parameters on the flow field.

Edney's classification system was based on an externally generated planar oblique shock impinging on the bow shock generated by a cylinder. The location of the impingement point, or alternatively the angle of the externally generated shock, determines the type of shock interaction that occurs. With double-wedge geometries, the first wedge generates the impinging shock, and the second wedge generates either a second oblique shock or a curved bow shock. The resulting interactions between these shock waves can be classified according to Edney's scheme. Four of the six interactions that Edney classified appear. However, because of geometrical constraints, there are differences between these four interactions on the different geometries, and a previously unidentified shock interaction is seen. Additionally, the different constraints imposed by the double-wedge geometry produce large-amplitude steady-state variations in surface pressure for certain interactions. The type of interaction that occurs depends on the relevant non-dimensional parameters, which for inviscid flow are the Mach number M, the ratio of specific heats γ, the ratio of the first wedge face length to the second wedge face length L_2/L_1, and the two wedge angles θ_1 and θ_2.

After a brief description of the numerical method, the details of double-wedge shock interactions are described in order of occurrence as the second wedge angle is increased. This is analogous to considering different oblique shock impingement points on a blunt body geometry such as the cylinder used by Edney. Emphasis is placed on the detailed structure of the interactions and the transition criteria between the various interactions. The discussion is split into two sections considering high and low Mach number flows separately. This is done because for a given first wedge angle and ratio of specific heats, there is a critical free-stream Mach number which determines the behavior of the flow along the wedge surface and, in turn, the basic structure of the interactions. This concept is described in detail below. The first wedge angle, ratio of wedge face lengths, and ratio of specific heats are held constant so that we can fully explore the remaining M, θ_2 parameter space.

2. Numerical method

The two-dimensional compressible Euler equations are solved using a finite-volume computational fluid dynamics method. The fluxes across cell surfaces are computed

https://doi.org/10.1017/S0022112097007131 Published online by Cambridge University Press

using a second-order-accurate upwind flux-vector splitting method (MacCormack & Candler 1989). The method has been used to simulate a wide variety of inviscid and viscous supersonic and hypersonic flows.

The boundary conditions for these inviscid flows are straightforward. Because the free stream is supersonic the inflow conditions are specified, and the grid is chosen so that the outflow is also supersonic. Thus, simple zeroth-order extrapolation of the variables at the outflow is appropriate. At the wedge surfaces, we force the normal-direction velocity to be zero and the surface normal-direction pressure gradient is set to zero.

It is critical to resolve the shock interaction regions in these double-wedge flows. Even though these flows are inviscid, the grid spacing introduces a length scale that determines the thickness of the shock waves. Therefore, it is important to use a grid that is sufficiently fine so that the implied length scale is much smaller than any relevant physical length scale, such as the length of a transmitted shock. The structure of the grid, particularly around the triple points, can alter the angles of the shock waves and contact surfaces. We have taken care to design grids with enough points in the proper locations to give the correct results. Based on the results of a grid resolution study (Olejniczak, Wright & Candler 1996), grid sizes of 512×512 points resolve all the relevant features in the flow fields. For some of the interactions, smaller sized grids predict the wrong type of interaction because of incorrect shock locations or shock angles. We decided to use grid sizes of 1024×1024 for all of the computations, ensuring that even the smallest-scale structures are resolved. This large grid size results in the highest quality solutions which can be achieved in a reasonable amount of computer time. Because of the large number of grid points required, these calculations were performed on the massively parallel Thinking Machines CM-5 using the Data-Parallel Lower-Upper Relaxation (DP-LUR) (Candler, Wright & McDonald 1994) implicit method to efficiently reach the steady-state solution.

3. Shock polar diagrams

It is useful to present shock interaction flows using pressure-deflection or (p, θ)-shock polar diagrams, in which the pressure jump across a shock wave is plotted versus the flow deflection angle. Following the conventions used by Edney, we present shock polars in which positive angles correspond to clockwise deflections from the horizontal and the path of the interaction is shown in bold.

Briefly, the shock polar represents the locus of all flow states that can be obtained by passing through a shock of the given Mach number. The entire region behind a planar shock wave is then represented by a single point on a (p, θ) diagram. The maximum angle that a flow can be turned by an oblique shock is easily seen: this is the point of maximum deflection which separates the polar into the weak and strong regions. Just below this point on the shock polar is the sonic point. Above the sonic point lie solutions which produce subsonic flow behind the oblique shock, and below this point lie solutions which produce supersonic flow behind the oblique shock. While the shock polar representation can be used to predict certain types of shock interactions, it is only an approximate representation of the flow in cases which have curved shock waves. In this situation, the shock polar is correct only in the vanishingly small region about the shock intersection point.

https://doi.org/10.1017/S0022112097007131 Published online by Cambridge University Press

4. Results

In this study we have restricted ourselves to $\gamma = 1.4$, $L_2/L_1 = 1$, and $\theta_1 = 15°$, which allows us to fully explore the two-dimensional M, θ_2 parameter space. The shock interactions are presented in order of occurrence as the second wedge angle increases. The discussion is split into subsections considering interactions above and below a critical Mach number which determines the behaviour of the flow that is downstream of the interaction region and along the wedge surface. The definition of the critical Mach number and the distinction between these two regimes will be clarified in the following discussion.

4.1. *High Mach number interactions*

In this subsection we present the results for inviscid double-wedge flows at $M = 9$. These results are characteristic of shock interactions that occur above the critical Mach number. After presenting the Mach 9 results, we discuss the effect of varying the Mach number on the type of interaction that occurs.

4.1.1. *Type VI interactions*

Figure 1 shows the computed pressure and Mach contours for a flow at $M = 9$ with wedge angles of $\theta_1 = 15°$ and $\theta_2 = 35°$. This flow is purely supersonic and has a shock interaction that corresponds to an Edney Type VI shock interaction. The attached oblique shock from the nose intersects the attached oblique shock from the corner of the wedges. A contact discontinuity separates the fluid that has passed through both oblique shocks from the fluid that has passed only through the oblique shock from the second wedge. The contact discontinuity can be clearly seen in the Mach contours. An expansion fan is emitted from the intersection point and reflects off the surface of the second wedge. The reflected expansion waves are deflected as they pass through the contact discontinuity emanating from the shock intersection point, and intersect with and weaken the oblique shock. The waves are also partially reflected from the contact discontinuity, as shown by the closed pressure contour on the second wedge, and recompress the fluid along the surface of the second wedge as indicated by the presence of the pressure contour which originates two-thirds of the way along the second wedge and by the presence of the closed Mach contour on the second wedge.

This is a standard interaction that occurs when two oblique shocks of the same family intersect, however the geometrical constraints imposed by the second wedge surface create the reflected expansion and compression waves which slightly complicate the flow. Two shocks are said to be in the same family if the flow behind both shocks is deflected either in the positive or negative direction.

A schematic drawing of this Type VI interaction is shown in figure 2, and the idealized interaction point is shown in close-up. The numbered regions correspond to the numbered points in the shock polar diagram of this interaction, which is shown in figure 3. Since the flow angle in Region (1) must be equal to the first wedge angle, Point (1) is on the $M = 9$ free-stream shock polar at the location $\theta = -15°$ (using Edney's angle convention). With the pressure ratio now fixed, the Mach number in Region (1), $M_1 = 5.04$, is uniquely determined, and the shock polar for Region (1) can be drawn originating from Point (1). Likewise, the flow in Region (2) must be parallel to the second wedge, and therefore Point (2) is located on the $M = 5.04$ polar at $\theta = -35°$. The location of Points (3) and (4) can also be determined from compressible gas-dynamic considerations: Point (4) must lie on the $M = 9$ polar; Point (3) must be at the same location as Point (4) because Regions (3) and (4) are

https://doi.org/10.1017/S0022112097007131 Published online by Cambridge University Press

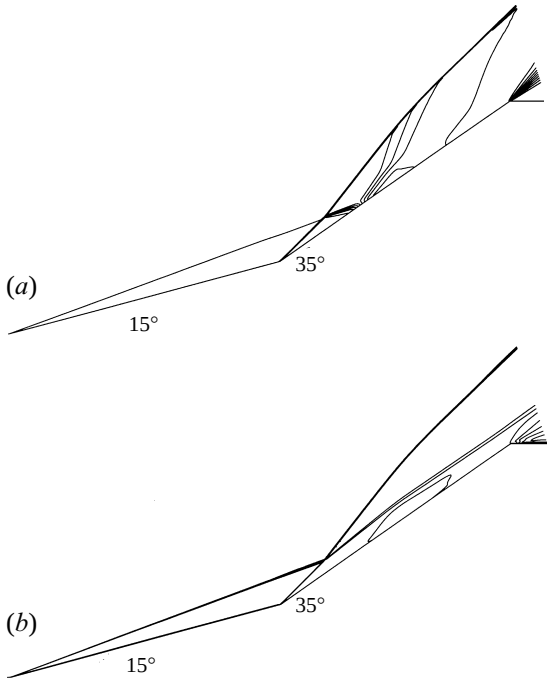


FIGURE 1. (*a*) Pressure contours for a Type VI interaction, and (*b*) Mach contours for a Type VI interaction, with $\theta_1 = 15°$, $\theta_2 = 35°$, $M = 9$, and $\gamma = 1.4$.

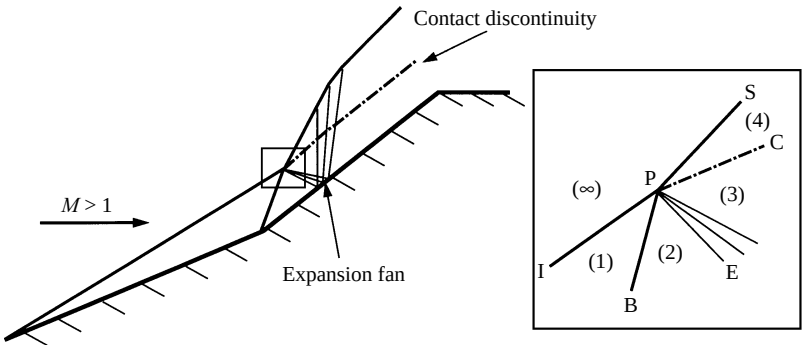


FIGURE 2. Schematic diagram of a Type VI shock interaction with an enlargement of the interaction region.

separated by a contact discontinuity; and Regions (2) and (3) must be connected by a Prandtl–Meyer expansion fan since the flow in Region (3) is underexpanded with respect to the flow in Region (4). Therefore, Points (3) and (4) lie on the intersection of the isentropic expansion path originating at Point (2) and the $M = 9$ polar. In this case the numerical results can be checked analytically, and the computed shock angles and post-shock pressures agree with this analysis.

For the interaction shown in figures 1–3, Points (3) and (4) lie below the sonic point of the free-stream polar. As the second wedge angle increases, Point (2) moves up and to the left on the (p, θ) diagram, and eventually the isentropic expansion path originating from Point (2) intersects the free-stream polar above the sonic point,

https://doi.org/10.1017/S0022112097007131 Published online by Cambridge University Press

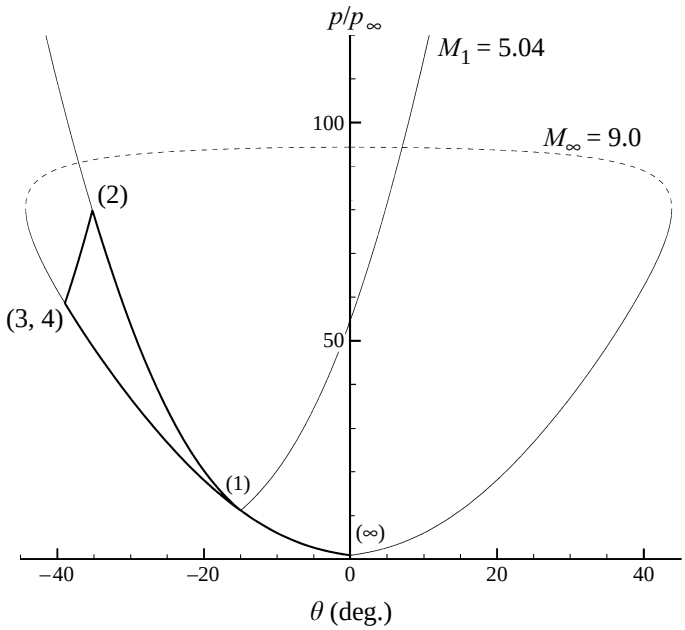


FIGURE 3. Shock polar diagram for a Type VI interaction with $\theta_1 = 15°$, $\theta_2 = 35°$, $M = 9$, and $\gamma = 1.4$.

and a purely supersonic Type VI interaction can no longer exist. Alternatively, it is equivalent to state that a purely supersonic Type VI interaction can no longer occur when a single weak oblique shock (PS in figure 2) cannot satisfy the matching conditions for Regions (3) and (4). This is the transition criterion between a Type VI and a Type V interaction, and it predicts transition at a second wedge angle of 39.76°, which is less than the maximum deflection angle of 44.16° for the free-stream flow. Previously, Bertin & Hinkle (1975) conducted a set of double-wedge experiments with a gap between the wedges in order to bleed the boundary layer and prevent separation. Their experimental results showed Type VI–Type V transition within 2° of the maximum deflection angle. However, it is possible that either the gap between the wedges or the viscous effects present in their experiment altered the transition point.

Our results also show that the transition process actually occurs continuously over a small range of second wedge angles, and not instantaneously at a discrete value of θ_2 as experiments seem to indicate. This transition mechanism is necessary as it is impossible for the three-shock Type VI configuration to jump directly to the seven-shock Type V configuration.

The transition from a Type VI to a Type V interaction is detailed in figure 4, which shows the pressure and Mach contours in the interaction region for a series of second-wedge angles. At an angle of 39.5°, there is still a purely supersonic Type VI interaction, with the isentropic expansion line intersecting the free-stream polar just below the sonic point on the polar. For a Mach 9 flow, the sonic point and the point of maximum deflection on the free-stream polar are separated by less than a hundredth of a degree and are essentially co-located. According to the method of characteristics, the transition criterion defined above predicts transition at a second wedge angle of $\theta_2 = 39.76°$. For second wedge angles up to 40.0°, strong Type VI

https://doi.org/10.1017/S0022112097007131 Published online by Cambridge University Press

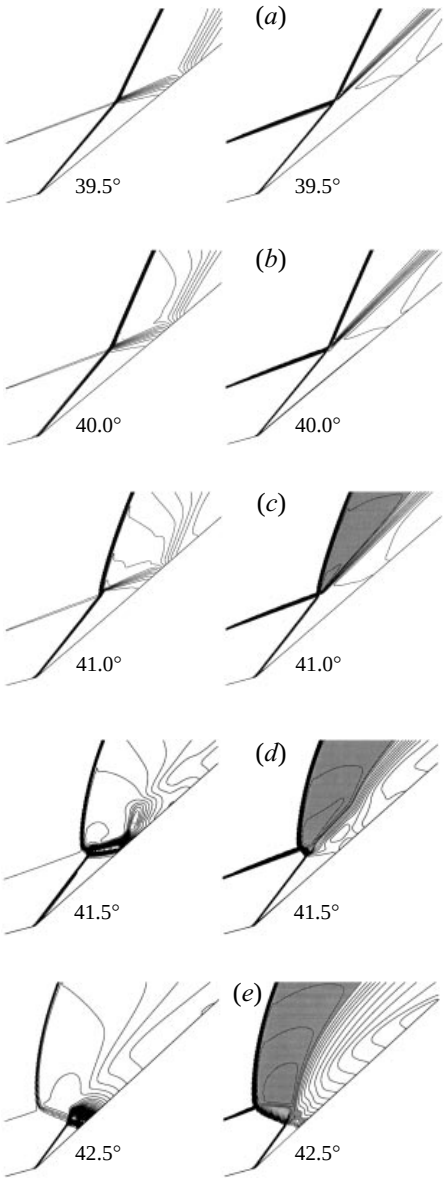


FIGURE 4. Pressure contours (left) and Mach contours (right) with the subsonic regions shaded for a series of second wedge angles, (*a*) 39.5°, (*b*) 40.0°, (*c*) 41.0°, (*d*) 41.5°, (*e*) 42.5°, showing the Type VI–Type V transition process. The first wedge angle is $\theta_1 = 15°$ with $M = 9$ and $\gamma = 1.4$.

interactions exist where the isentropic expansion path intersects the free-stream polar on the strong region of the curve. All of the shocks are still straight, but there is a small subsonic pocket near the triple point (P). Figure 4 shows this strong Type VI interaction for a second wedge angle equal to this maximum possible value of 40.0°. The subsonic region is so small that it is not visible in the figure; however it is present in the solution. For larger second wedge angles, it is impossible for the flow in Region (4) to be generated by a single oblique shock and still meet the required matching conditions with Region (3). Therefore, Shock PS becomes curved and there

https://doi.org/10.1017/S0022112097007131 Published online by Cambridge University Press

is an intermediate interaction that we call a supercritical Type VI. This is seen at $\theta_2 = 41.0°$. The subsonic region is considerably larger than in the strong Type VI interaction, but there is still the same basic three-shock pattern with an expansion fan. As the second wedge angle increases to 41.5° there is a sudden change in the flow structure. The oblique shock from the corner of the wedges interacts with a transmitted shock that emerges from the intersection of the nose shock and the bow shock. An expansion fan is still present, but it merges with a compression wave that strikes the second wedge. Finally, for $\theta_2 = 42.5°$ the full seven-shock structure of a Type V interaction is required turn the flow; this Type V interaction is discussed in detail in the next subsection. It is interesting to note that the maximum surface pressure jumps from a value of 110 times the free-stream value for the Type VI interaction to a value of 730 times the free-stream value for the Type V interaction within a range of second wedge angles that is less than 3°.

4.1.2. *Type V interactions*

The computed Mach contours for a Type V interaction with $\theta_2 = 45°$ are shown in figure 5. The flow structure is best explained by considering a schematic drawing (figure 6) of a Type V interaction. In the following discussion we relate the flow-field features shown in the schematic to the flow-field solution shown in figure 5. Because Shock PS is curved and the flow in Region (3) is non-uniform, Shock PT must also be curved. The curvature of this shock gives rise to a region of weak flow gradients originating behind the shock, bounded by the two contact discontinuities (C_1 and C_2) emitted from P and T. This forms what appears in numerical solutions and experiments as a thick contact surface, which is termed a jet by Edney. However, in figure 5(*c*), a plot of the entropy in the shock interaction region, it is possible to distinguish C_1 and C_2 from the regions of weak gradients (Regions 2 and 4) which they enclose. The streamlines which pass through the triple points show the location of the contact discontinuities. The entropy gradient in Region (2) is clearly visible in figure 5(*c*), and the presence of the resulting weak waves in the jet region between C_1 and C_2 can be seen from the sinuous shapes of C_1 and C_2 in figure 5(*a*).

The flow in Region (4) must match pressure and angle with the flow which passes through Shock TQ, necessitating Shock TU which separates Regions (2) and (4). This shock can also be seen in figure 5. It was foreseen by Edney and is shown on his shock polar, but was in fact never indicated in his schematic diagram. The inboard flow, defined as the flow which has passed through the oblique shock on the first wedge, remains supersonic as it is turned by Shock QB at the corner of the wedges and passes through Shock QR. In this case, Shock QR undergoes a regular reflection at the surface, although in the $\theta_2 = 42.5°$ case shown earlier, Shock QR undergoes a Mach reflection at the surface.

In the inboard flow region there is a series of alternating isentropic compression and expansion waves, similar to those that occur in an underexpanded jet. The appearance of an underexpanded jet impinging on the body is generally associated with a Type IV interaction and is explained in detail in the next subsection, but these results show that the jet is actually associated with the fact that the inboard flow downstream of the interaction region is underexpanded with respect to the outboard flow in the adjacent subsonic region. Mach waves from the underexpanded jet are partially transmitted as acoustic waves through the contact surface into the subsonic region. Because the pressure varies along the contact surface, these acoustic waves are non-uniform and produce the inflection points in the bow shock and the unusual shape of the sonic line that can be seen in figure 5(*a*).

https://doi.org/10.1017/S0022112097007131 Published online by Cambridge University Press

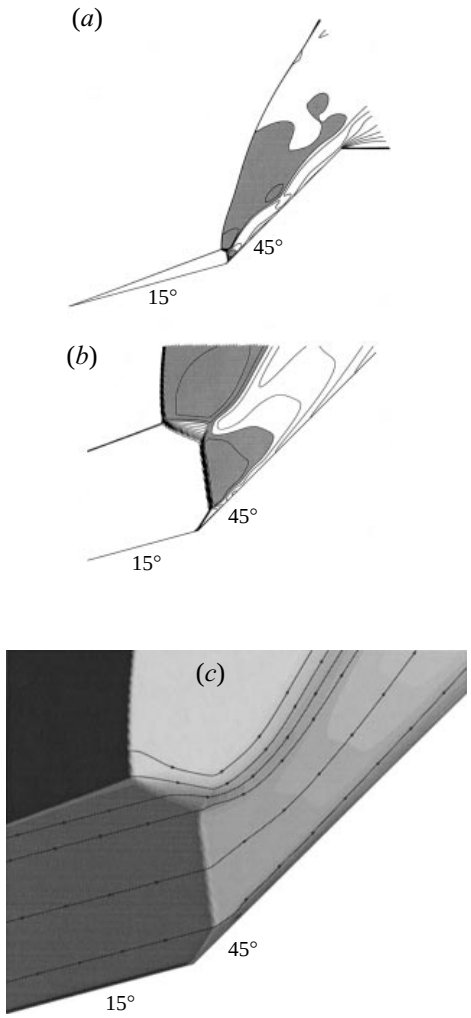


FIGURE 5. (*a*) Mach contours (subsonic region shaded) for a Type V interaction, (*b*) enlargement of the interaction region showing Mach contours (subsonic region shaded), and (*c*) enlargement of the interaction region showing streamlines with flooded entropy contours. The wedge angles are $\theta_1 = 15^\circ$ and $\theta_2 = 45^\circ$ with $M = 9$ and $\gamma = 1.4$.

Figure 7 shows the shock polar for a Type V interaction corresponding to figure 5, with the numbered regions corresponding to figure 6. Points (1) and (6) are located by the requirement that the flow angles match the first and second wedge angles, respectively; Points (2) and (3) must be co-located on the intersection of the free stream and Region (1) polars; Points (4) and (5) must be co-located on the intersection of the Region (1) and Region (2) polars; and likewise Points (7) and (8) must be co-located on the intersection of the Region (1) and Region (6) polars. The predictive capability of the shock polar can be judged by comparing the analytical pressure ratios with the computed surface pressure, shown in figure 8. The first peak in normalized surface pressure, at a value of 150.5, is due to the oblique shock at the corner and should be equal to the pressure ratio in Region (6). Point (6) on the shock polar diagram is at a value of 149.2, and the theory agrees reasonably well with the computation. The

https://doi.org/10.1017/S0022112097007131 Published online by Cambridge University Press

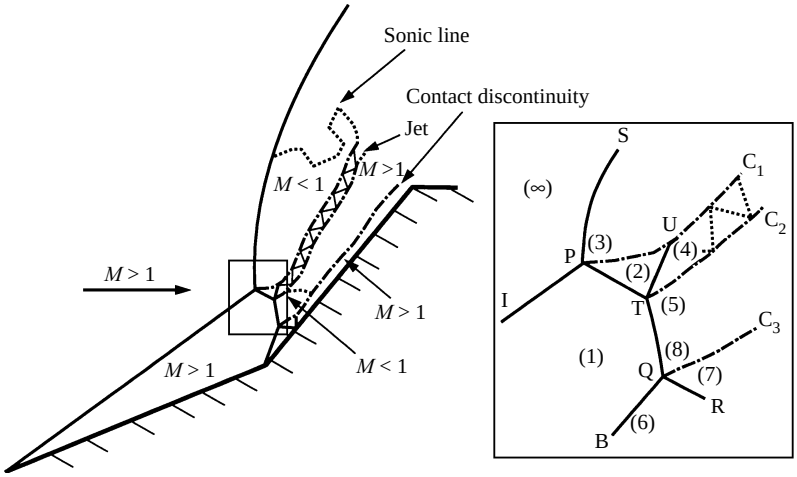


FIGURE 6. Schematic diagram of a Type V shock interaction with an enlargement of the interaction region.

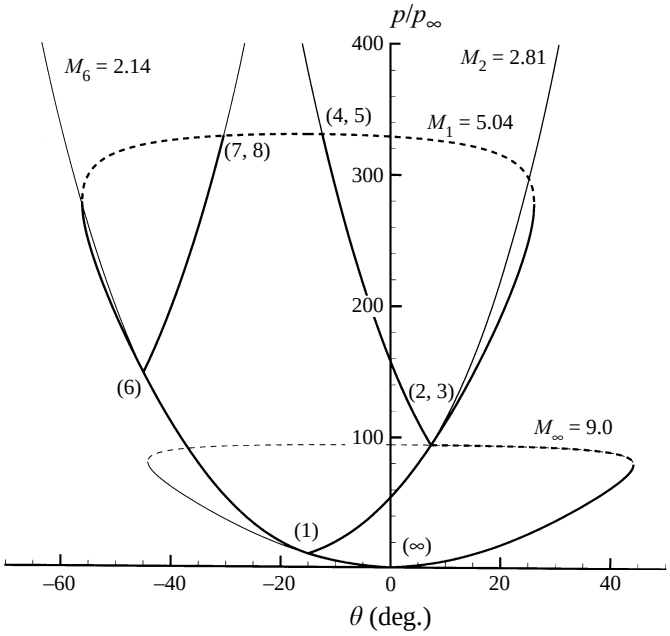


FIGURE 7. Shock polar diagram for a Type V interaction with $\theta_1 = 15°$, $\theta_2 = 45°$, $M = 9$, and $\gamma = 1.4$.

largest peak in computed surface pressure, at a pressure ratio of 520, is due to the regular reflection of Shock QR on the wedge surface. Using the shock jump relations, the predicted pressure ratio is 685; this difference is due to the presence of the curved shocks.

In contrast to the $\theta_2 = 42.5°$ case, Shock QR undergoes a regular reflection rather than a Mach reflection at the surface of the second wedge. The maximum surface pressure in this case is lower because of the different angle of incidence of Shock QR. There are three more pressure peaks before the corner of the second wedge due to the

https://doi.org/10.1017/S0022112097007131 Published online by Cambridge University Press

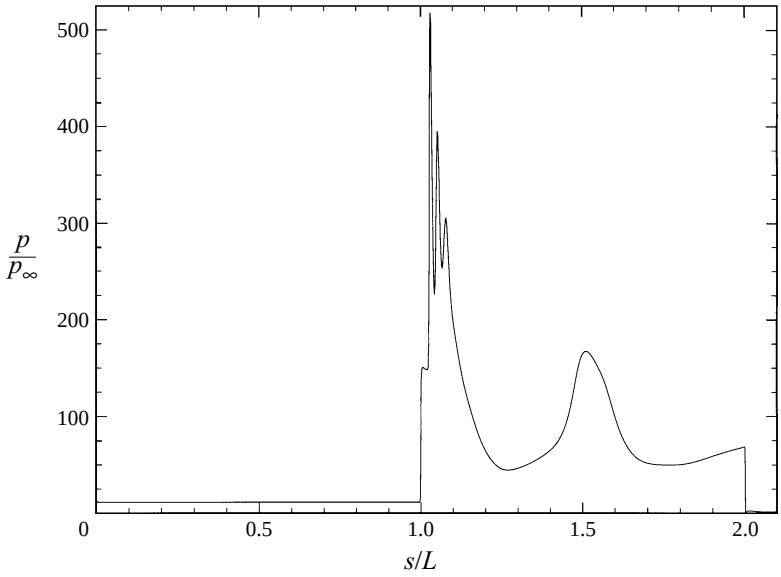


FIGURE 8. Surface pressure for a Type V interaction with $\theta_1 = 15°$, $\theta_2 = 45°$, $M = 9$, and $\gamma = 1.4$.

alternate compressions and expansions of the jet along the wall. The close spacing of these peaks near the corner demonstrates the need for highly resolved grids in order to accurately compute this interaction.

As the second wedge angle increases, the oblique corner shock QB shortens, until it becomes impossible to match the imposed pressure conditions with an attached oblique shock. At this point, Shock QB disappears, Shock TQ impinges on the first wedge, and a Type IV interaction occurs. The second wedge angle at which transition occurs cannot be computed analytically owing to the curved shocks and subsonic flow regions. Numerical computations indicate that the flow transitions to a Type IV interaction at a second wedge angle that is much smaller than the relative maximum flow deflection angle for Region (1), owing once again to the imposed pressure condition which must be met by the inboard flow. For these conditions the largest second wedge angle which produces a Type V interaction is 45.25°, while the relative maximum flow deflection angle is 56.18°. Again, this is a different transition criterion than expected and observed by Bertin & Hinkle (1975), who reported transition for second wedge angles within 2° of the maximum deflection angle for the flow adjacent to the first wedge. This is not surprising as the gap between the wedges in their experiment alters the Type V–Type IV transition process.

4.1.3. *Type IV interactions*

Figure 9 is a plot of the pressure contours for a Type IV interaction with $\theta_2 = 50°$. Large amplitude variations in the steady-state pressure are clearly visible along the surface of the second wedge. The interaction is so close to the corner that the compression due to the normal shock and the compression due to the corner result in a nearly constant pressure near the corner region. After the pressure peak at the corner, alternating pressure minima and maxima are visible along the second wedge surface, as visualized by the rounded contours centred at the extrema locations. The peak pressure occurs at the corner and is about 360 times the free-stream value, which is lower than the peak pressure for the Type V interaction discussed earlier.

https://doi.org/10.1017/S0022112097007131 Published online by Cambridge University Press

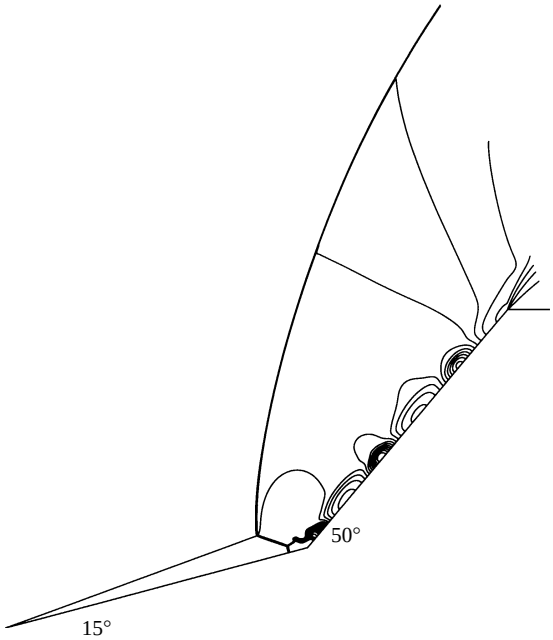


FIGURE 9. Pressure contours for a Type IV interaction with $\theta_1 = 15°$, $\theta_2 = 50°$, $M = 9$, and $\gamma = 1.4$.

Figure 10 shows the Mach contours and the streamlines with flooded entropy contours in the region of the triple point. A sinuous contact discontinuity originates from the triple point, as is apparent from the value of the entropy and the streamlines. The reason for the shape of the contact discontinuity is as follows. The fluid passing through the bow shock PS (see figure 11, a schematic of a Type IV interaction) just above the triple point is deflected towards the body, causing the supersonic fluid in Regions (2) and (4) to be compressed. This supersonic fluid forms a jet which is underexpanded with respect to the adjacent subsonic fluid in Regions (3) and (5). The jet undergoes alternate compressions and expansions which produce the waviness of the contact discontinuity and the resulting pressure variations along the entire length of the second wedge. These variations are a result of the reversible exchange of kinetic and internal energy due to the $p\nabla \cdot \boldsymbol{u}$ term appearing with opposite sign in the kinetic and internal energy equations. This is analogous to the classic problem of an underexpanded jet exhausting into stagnant air. However, there are fundamental differences which produce the unique characteristics of the double-wedge flows. The jet is trapped against the wedge surface for much of its extent, and the imposed pressure condition at the edge of the jet is not constant, resulting in curved Mach waves in the jet and a series of smooth, rounded variations. Additionally, the flow in Regions (3) and (5) surrounding the jet is not stagnant, and thus non-uniform transmission of acoustic waves into this subsonic flow is required to satisfy the flow tangency condition along the contact surfaces. These results are similar to those of Lamont & Hunt (1980), who studied underexpanded jets impinging on inclined plates. They also observed steady variations in the measured surface pressure.

The shock polar for a Type IV interaction with $\theta_1 = 15°$ and $\theta_2 = 50°$ is shown in figure 12. This shock polar is much simpler than the Type V polar. Effectively, Regions (6), (7), and (8) from the Type V flow field disappear and the contact surface C_3 is replaced by the surface of the double wedge. Region (5) is bounded by the first

https://doi.org/10.1017/S0022112097007131 Published online by Cambridge University Press

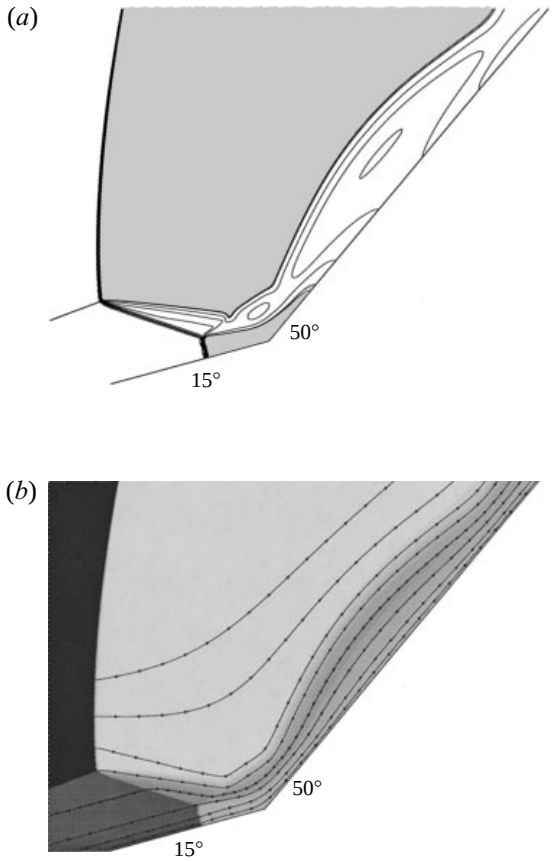


FIGURE 10. Enlargement of the interaction region for a Type IV interaction showing (*a*) Mach contours (subsonic region shaded), and (*b*) streamlines with flooded entropy contours. The wedge angles are $\theta_1 = 15^\circ$ and $\theta_2 = 50^\circ$ with $M = 9$, and $\gamma = 1.4$.

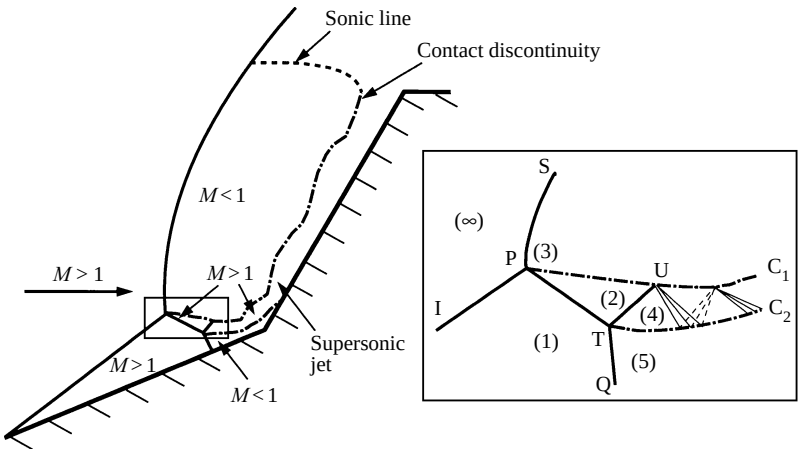


FIGURE 11. Schematic diagram of a Type IV shock interaction with an enlargement of the interaction region.

https://doi.org/10.1017/S0022112097007131 Published online by Cambridge University Press

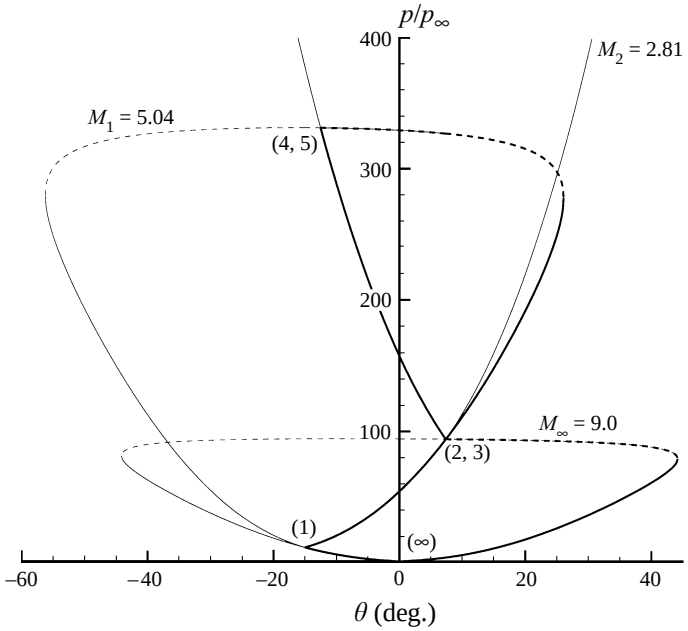


FIGURE 12. Shock polar diagram for a Type IV interaction with $\theta_1 = 15°$, $\theta_2 = 50°$, $M = 9$, and $\gamma = 1.4$.

wedge surface, and therefore Shock TQ must be curved to match the flow tangency conditions at the contact surface C_2 and on the wedge surface. These shock curvature effects have a major impact on the flow field, as discussed above, and cannot be predicted by the shock polar diagram.

As the second wedge angle increases further, the triple point moves towards the nose of the first wedge and the flow just above the triple point in Region (3) is deflected less towards the body as the oblique nose shock impinges on the bow shock nearer and nearer to the point of zero curvature of the bow shock. This means that the flow in Region (2) is deflected less towards the body, and there is a point at which a regular reflection rather than a Mach reflection occurs. Region (5) in the Type IV interaction then disappears and the flow in Region (4) is determined by the flow tangency condition on the first wedge. This is the transition criterion between a Type IV interaction and a new type of shock interaction that does not fit into Edney's classification scheme. In fact, this type of interaction cannot occur for the types of blunt body flows Edney investigated, as it is only possible for specific orientations of the geometry surface with respect to the interaction point. We refer to this interaction as a Type IVr.

4.1.4. *Type IVr interactions*

The Mach contours for a Type IVr interaction with $\theta_2 = 60°$ are shown in figure 13. The variations in Mach number and surface pressure now extend from halfway up the first wedge to the end of the second wedge, and are more pronounced than in any of the previous cases. As can be seen in figure 13(*b*), the inboard flow is entirely supersonic after the interaction region. However, a normal shock must occur just before the corner because the angle that the inboard flow must turn is greater the maximum possible deflection angle. The flow downstream of the corner quickly re-accelerates to supersonic speed. The interaction region is similar to the region shown

https://doi.org/10.1017/S0022112097007131 Published online by Cambridge University Press

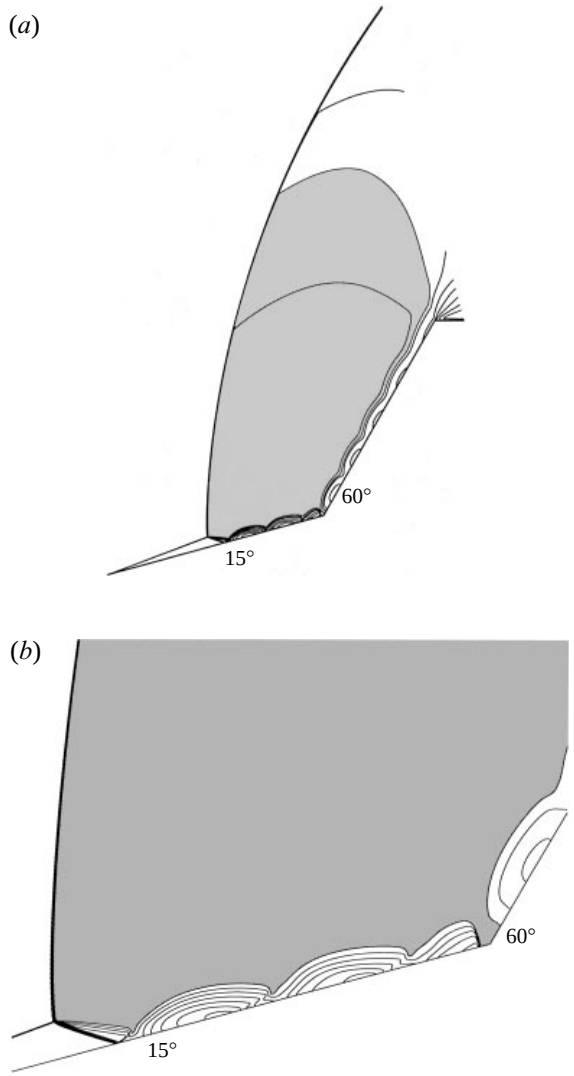


FIGURE 13. (*a*) Mach contours (subsonic region shaded) for a Type IVr interaction, and (*b*) enlargement of the interaction region. The wedge angles are $\theta_1 = 15^\circ$ and $\theta_2 = 60^\circ$ with $M = 9$, and $\gamma = 1.4$.

in figure 10 for the Type IV interaction, but the fluid passing through the oblique shocks is more highly compressed. This can be seen in figure 14, which shows the surface pressure for this case. The first peak, due to the regular reflection of the transmitted shock PT off the first wedge, is 430 times the free-stream pressure, which is higher than the peak of the Type IV interaction. This peak is followed by a region of underexpanded isentropic flow until the normal shock just before the corner. The heights of the two pressure peaks in this region are controlled by the area of the jet, which is determined by the pressure and flow direction in the subsonic region immediately above it. The maximum surface pressure of 450 times the free-stream pressure is due to the normal shock at the corner. Finally, there are four pressure maxima along the second wedge due to the alternating isentropic expansions and compressions in the supersonic jet.

https://doi.org/10.1017/S0022112097007131 Published online by Cambridge University Press

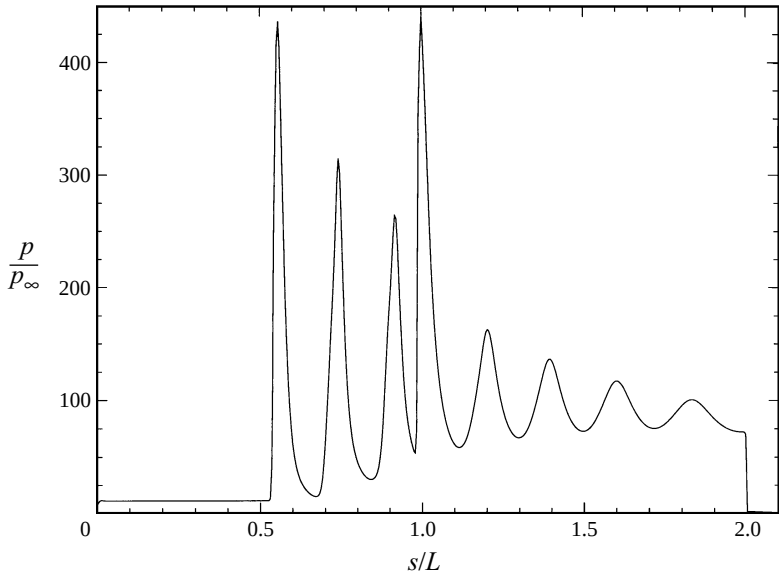


FIGURE 14. Surface pressure for a Type IVr interaction with $\theta_1 = 15°$, $\theta_2 = 60°$, $M = 9$, and $\gamma = 1.4$.

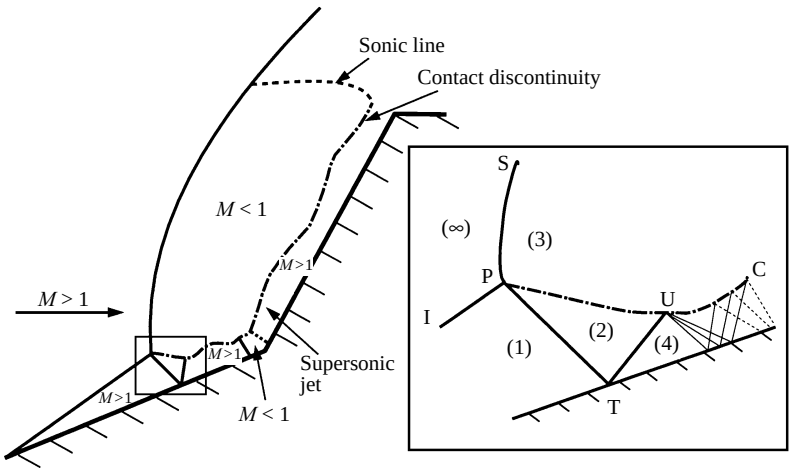


FIGURE 15. Schematic diagram of a Type IVr shock interaction with an enlargement of the interaction region.

The schematic of a Type IVr interaction is shown in figure 15. The numbered regions correspond to the points on the shock polar diagram (figure 16) with $\theta_2 = 60°$. As can be seen, the only difference between this shock polar and the Type IV polar is the location of Point (4). In the Type IV interaction, the location of Point (4) is determined by the fact that it must be co-located with Point (5). In the Type IVr interaction, Point (4) must be located on the Region (2) polar at the point $\theta = -15°$. In both cases, Points (2) and (3) are determined from the free-stream Mach number and the first wedge angle; there is no effect of the second wedge angle on either the Type IV or the Type IVr shock polar diagram. But once again, owing to curved shock

https://doi.org/10.1017/S0022112097007131 Published online by Cambridge University Press

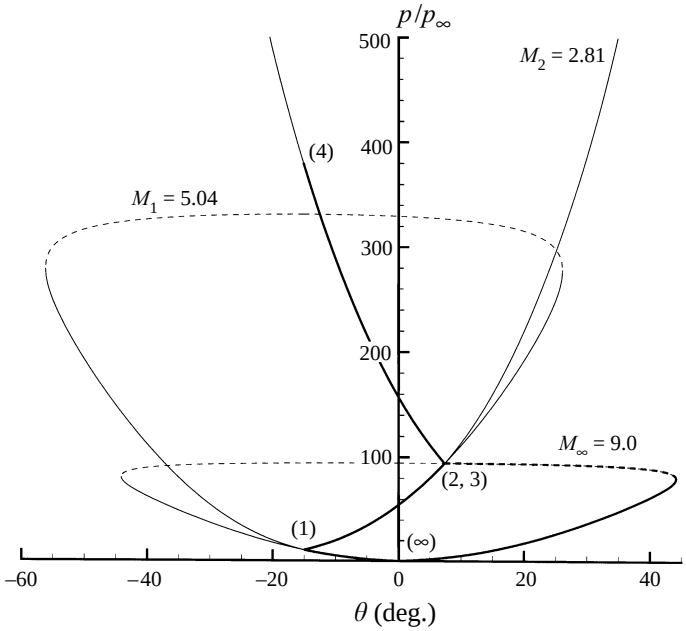


FIGURE 16. Shock polar diagram for a Type IVr interaction with $\theta_1 = 15°$, $\theta_2 = 60°$, $M = 9$, and $\gamma = 1.4$.

effects, the predicted pressure ratio in Region (4) of 375 on the shock polar diagram is less than the computed value of 430.

Because the Type IV–Type IVr transition depends on the curvature of the bow shock near Point P, which depends on the second wedge angle, it is impossible to use the shock polar diagram to predict the Type IV–Type IVr transition. In fact, for these conditions the Type IV–Type IVr transition occurs in the regime where the shock polars show that both a regular reflection and a Mach reflection are possible. Considering the Type IV and Type IVr polars, figures 12 and 16 respectively, the Region (2) polar intersects both the Region (1) polar and the line $\theta = -15°$. Both of these intersection points represent possible flow states for Region (4), and the polars show that this is the dual solution regime where either a Mach reflection (Type IV interaction) or a regular reflection (Type IVr interaction) is possible.

Since transition occurs in the dual regime, neither the von Neumann condition nor the detachment condition can be used to determine when transition occurs. The von Neumann condition implies that if the Region (2) polar intersects the strong portion of the Region (1) polar, a Mach reflection will occur. The detachment condition implies that a regular reflection will occur if the Region (2) polar intersects the line $\theta = -15°$. Clearly neither of these criteria apply to the Type IV–Type IVr transition on a double-wedge geometry, because the transition depends on the pressure distribution downstream of the interaction point as determined by the second wedge angle.

As the second wedge angle increases and the impingement point of the nose shock on the bow shock moves closer to the nose of the first wedge, there are two effects. First, the oblique shock from the nose of the first wedge impinges closer to the point of zero curvature on the bow shock, resulting in less downward streamline deflection beyond the triple point. This produces a lower pressure at the edge of the supersonic region adjacent to the body and reduces the strength of the reflected shock at the

https://doi.org/10.1017/S0022112097007131 Published online by Cambridge University Press

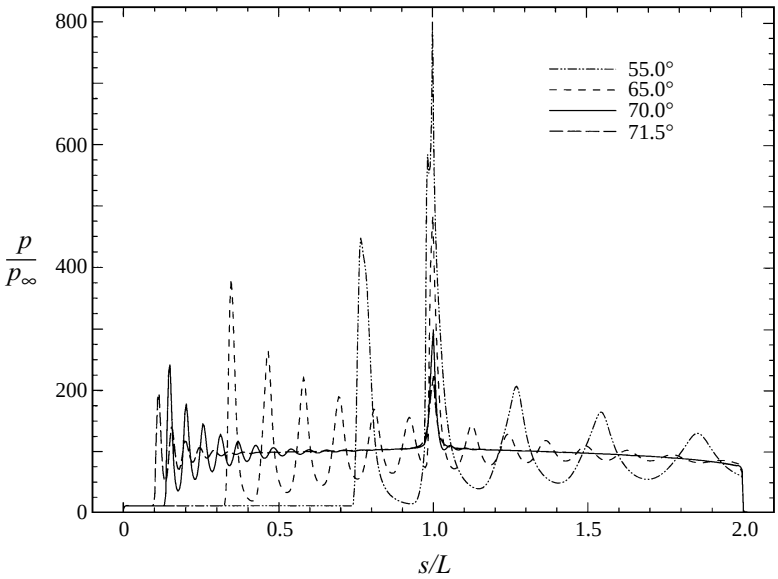


FIGURE 17. Surface pressure for a series of Type IVr interactions with $\theta_1 = 15°$, $M = 9$, and $\gamma = 1.4$.

surface of the first wedge. This in turn reduces the first maximum in surface pressure and the amount of underexpansion in the supersonic jet. Second, Points P and U in figure 15 move closer to the wedge surface, effectively decreasing the jet area and producing shorter peak-to-peak distances for the pressure maxima because the waves have less distance to travel between reflections. This can be seen in figure 17, which plots the surface pressure for a series of Type IVr interactions with increasing second wedge angle. The limiting case is when Point P is at the nose of the wedge, and the bow shock is at the point of detaching. For this case there is no downward streamline deflection, and the post-bow-shock pressure on the surface is the normal shock jump value for the free-stream Mach number, which is 94 times the free-stream pressure for this case. This flow can be thought of as perfectly expanded. The surface pressure is nearly constant until it increases at the corner of the wedges. The pressure then decreases to approximately the normal shock jump value by the end of the second wedge.

4.1.5. *Transition criteria*

The transition criteria discussed above can be summarized on a parametric diagram of Mach number versus second wedge angle, shown in figure 18. The Type VI to Type V transition line is determined analytically from the method of characteristics, and predicts transition for significantly lower second wedge angles than the maximum deflection angle criterion. The reason for this lower transition angle can be seen by considering figure 2. The expansion fan between Regions (2) and (3) turns the flow counter-clockwise so that the angle of the contact discontinuity at the triple point is larger than the second wedge angle. Therefore, the flow in Region (4) must have turned by an angle greater than the second wedge angle. Thus, transition occurs when the flow in Region (4) reaches the maximum deflection angle. The actual transition process occurs over a range of second wedge angles, and the computations agree with this analytical criterion in the sense that pure supersonic Type VI interactions cease to exist for the predicted second wedge angle.

The Type V to Type IV transition line cannot be determined analytically, owing to

https://doi.org/10.1017/S0022112097007131 Published online by Cambridge University Press

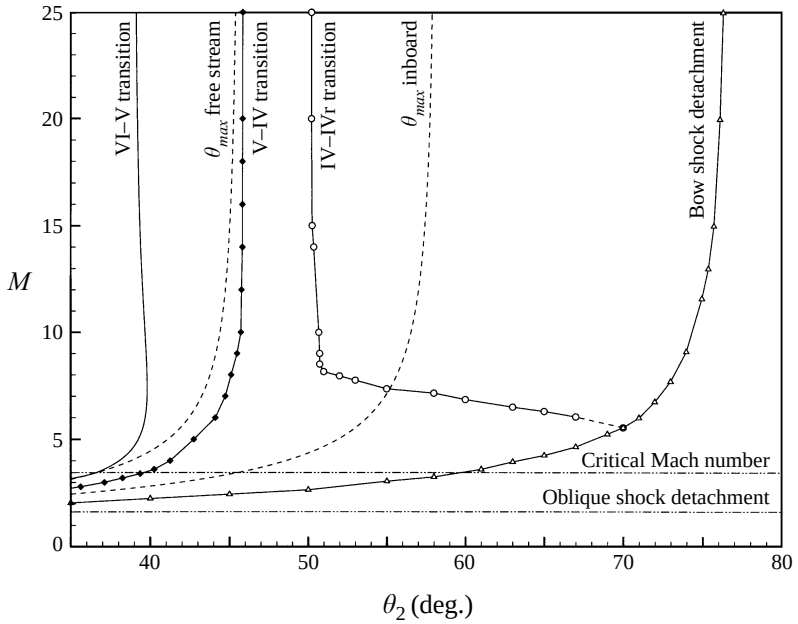


FIGURE 18. Diagram of Mach number vs. second wedge angle showing the regimes of the different interactions for high Mach number flows. $\theta_1 = 15°$, $\gamma = 1.4$, $L_2/L_1 = 1$.

the subsonic flow and curved shocks present, and must be computed. Each symbol on this curve represents a numerically determined point. It can be seen that the flow transitions to a Type IV interaction very quickly after the maximum deflection angle for the free stream, and well before the maximum deflection angle with respect to the flow inboard of the nose shock. The Type IV to Type IVr transition line has a strong Mach number dependence. For high Mach number flow (above Mach 8) transition occurs at about 50.5°. As the Mach number decreases below this point, the transition to a Type IVr interaction is rapidly delayed, and in fact does not occur at all below Mach 5.5, as it is no longer possible to have a regular reflection at the surface of the first wedge. This transition line also must be determined numerically.

The curved line marked 'Bow shock detachment' signifies when the triple point reaches the nose of the first wedge and the bow shock detaches, resulting in a single bow shock rather than a shock interaction. The lower horizontal line at Mach 1.61 labelled 'Oblique shock detachment' represents the Mach number below which the nose shock will always be detached on the 15° first wedge.

The horizontal line at Mach 3.43 labelled 'Critical Mach number' marks the distinction between the high and low Mach number regimes. Above this critical Mach number the inboard flow downstream of the interaction region is always underexpanded, as described above. Below the critical Mach number it is possible to have either overexpanded or underexpanded flows, as described in the next subsection. This is the basis for separating the discussion into high and low Mach number regimes. The value of the critical Mach number can be calculated analytically and depends on γ and θ_1, but it is independent of θ_2, as shown in figure 18.

4.2. *Low Mach number interactions*

In this subsection we present the results for inviscid double-wedge flows at $M = 2.8$ with varying second wedge angles. These results are characteristic of shock interactions

https://doi.org/10.1017/S0022112097007131 Published online by Cambridge University Press

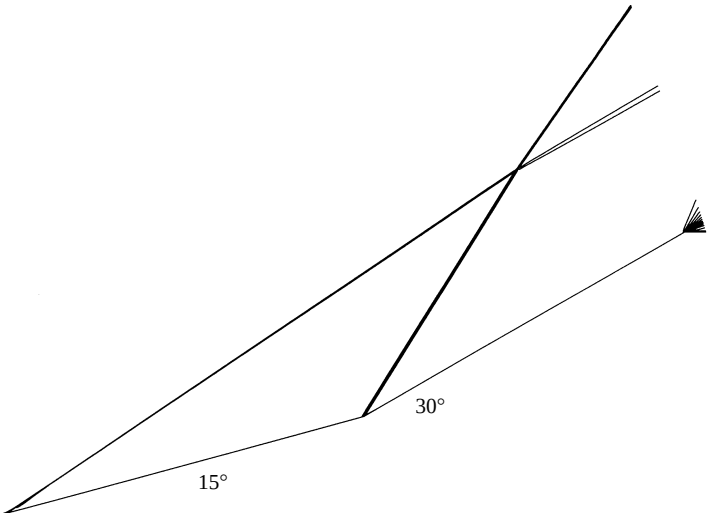


FIGURE 19. Mach contours for a Type VI interaction with $\theta_1 = 15°$, $\theta_2 = 30°$, $M = 2.8$, and $\gamma = 1.4$.

that occur below the critical Mach number. The effect of varying the Mach number is discussed at the end of the subsection. As these low Mach number interactions are in many respects similar to the high Mach number interactions, only the differences between them are discussed in detail.

4.2.1. *Type VI interactions*

Figure 19 shows the Mach contours for a Type VI interaction with $\theta_2 = 30°$. Compared to the high Mach number case, this and all low Mach number Type VI interactions are only slightly underexpanded. The expansion fan is very weak and turns the flow through an angle of only 0.085°, corresponding to a pressure ratio of approximately 0.995. Therefore, the expansion fan cannot be seen in figure 19. However, the contact surface emanating from the interaction point is visible.

As the second wedge angle increases, the flow becomes less underexpanded, eventually reaching a point where it is perfectly expanded and there are no waves downstream of the shock interaction point. A further increase in the second wedge angle results in an overexpanded flow where the pressure must increase after the interaction region to match the outboard flow conditions. Referring to figure 3, the shock polar for a Type VI interaction, Point (2) moves below Points (3) and (4), and a shock replaces the expansion fan that is present in the Type VI interaction. This is now a Type I interaction, which in this context can be thought of as an overexpanded Type VI interaction.

4.2.2. *Type I interactions*

The four-shock Type I interaction is common when two shocks of different families intersect, but only rarely occurs after the intersection of two shocks from the same family. A schematic drawing of a Type I interaction is shown in figure 20. The only difference between this Type I interaction and the Type VI interaction shown in figure 2, is that an oblique shock (PR) has replaced the expansion fan (PE). For double-wedge flows all Type I interactions are only very weakly overexpanded. This can be seen in figure 21 which shows the shock polar for a Type I interaction with $M = 2.8$ and $\theta_2 = 32.5°$. Point (2) is at the location $\theta = -32.5°$ on the Region (1)

https://doi.org/10.1017/S0022112097007131 Published online by Cambridge University Press

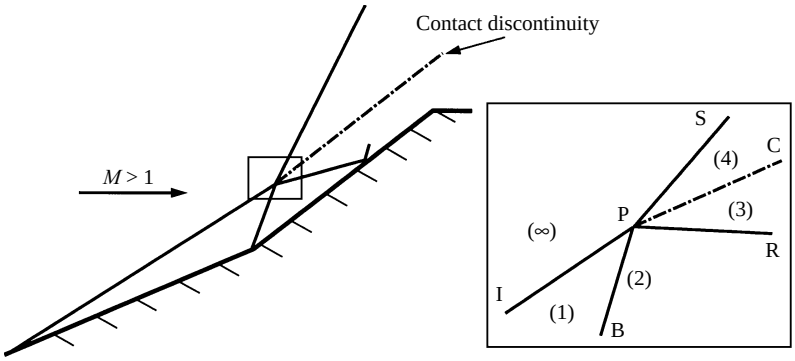


FIGURE 20. Schematic diagram of a Type I shock interaction with an enlargement of the interaction region.

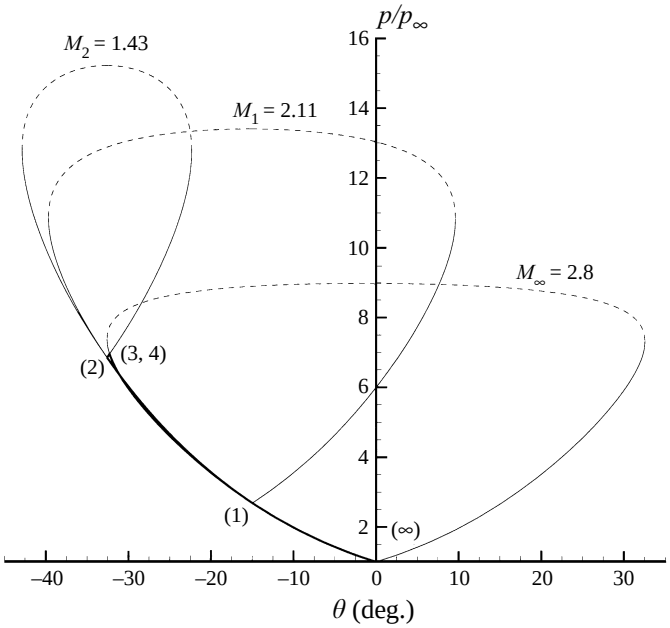


FIGURE 21. Shock polar diagram for a Type I interaction with $\theta_1 = 15°$, $\theta_2 = 32.5°$, $M = 2.8$, and $\gamma = 1.4$.

polar, while Points (3) and (4) are on the intersection of the free-stream polar with the Region (2) polar. The pressure in Region (3) is only 1.014 times greater than the pressure in Region (2). The perfectly expanded case occurs when the free-stream polar and the Region (1) polar intersect. This occurs at $\theta_2 = 31.08°$ for Mach 2.8 flow. In the perfectly expanded case Points (2), (3), and (4) are co-located.

In the low Mach number regime, Type I interactions transition to Type V interactions. The Type I–Type V transition process is similar to the Type VI–Type V transition process that occurs at high Mach numbers. In this case the four-shock Type I configuration changes to the seven-shock Type V configuration over a range of second wedge angles.

https://doi.org/10.1017/S0022112097007131 Published online by Cambridge University Press

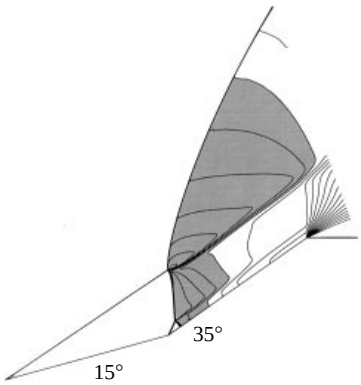


FIGURE 22. Mach contours (subsonic region shaded) for a Type V interaction with $\theta_1 = 15°$, $\theta_2 = 35°$, $M = 2.8$, and $\gamma = 1.4$.

4.2.3. *Type V interactions*

While by definition the low Mach number Type V interaction has the same shock polar as the high Mach number case, the flow field downstream of the interaction point is significantly different. This can be seen in figure 22, which shows the Mach contours for a Type V interaction with $\theta_2 = 35°$. Compared to the high Mach number case, Shock TU in figure 6 is much smaller and cannot be distinguished in figure 22. However a small supersonic region exists, as evidenced by the shock polar for this interaction. Since Shock TU is vanishingly small for this case, the two contact surfaces C_1 and C_2 that bound the jet in the high Mach number flow merge into the jet-like feature that Edney identified. It can be seen in figure 22 that this jet does not impinge on the body. Additionally, the flow is subsonic after the normal shock that strikes the second wedge. This is analogous to an overexpanded nozzle, where a normal shock forms inside the nozzle in order to match the downstream pressure condition. The pressure decreases smoothly along the second wedge after the normal shock, with the flow re-accelerating to supersonic speed. The Type V–Type IV transition criterion is the same as in the high Mach number regime.

4.2.4. *Type IV interactions*

The Mach contours for a Type IV interaction with $\theta_2 = 38°$ are shown in figure 23. Compared to the high Mach number Type IV interaction shown previously in figure 11, Shock PT nearly disappears, and the underexpanded jet that is such a prominent feature of the typical Type IV shock interaction becomes a shear layer which does not impinge on the body. The computed flow field behind Shocks PS and TQ is subsonic, including the shear layer that separates them. However, if we examine the shock polar for this case we see that the flow in Region (2) must still be supersonic ($M_2 = 1.16$) until it passes through Shock TU, which is present in the calculation but because it is extremely small, it cannot be distinguished in figure 23. The subsonic flow downstream of the interaction is accelerated to supersonic speeds as it travels down the second wedge. Since a Type IVr interaction is impossible at this Mach number because a regular reflection cannot occur at the surface of the first wedge, the Type IV interaction is seen with increasing second wedge angle until the bow shock detaches from the nose.

https://doi.org/10.1017/S0022112097007131 Published online by Cambridge University Press

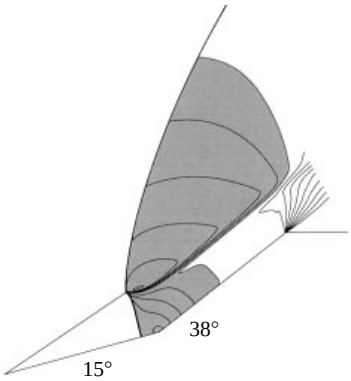


FIGURE 23. Mach contours (subsonic region shaded) for a Type IV interaction with $\theta_1 = 15°$, $\theta_2 = 38°$, $M = 2.8$, and $\gamma = 1.4$.

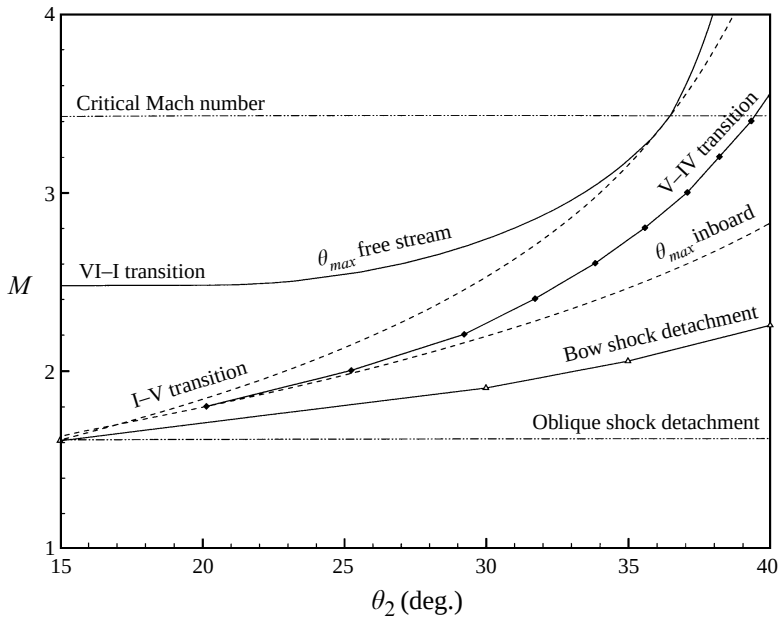


FIGURE 24. Diagram of Mach number vs. second wedge angle showing the regimes of the different interactions for low Mach number flows. $\theta_1 = 15°$, $\gamma = 1.4$, and $L_2/L_1 = 1$.

4.2.5. *Transition criteria*

Figure 24 shows the low Mach number regime of the M, θ_2 diagram. For small second wedge angles and high Mach numbers, a Type VI interaction occurs. In this region of the parameter space, the inboard flow downstream of the interaction is underexpanded. The Type VI–Type I transition line represents the locus of flow states for which the flow is perfectly expanded. Below this line, the flow is overexpanded and Type I interactions occur.

The Type I–Type V transition occurs at a second wedge angle equal to the maximum deflection angle for the free stream, because for second wedge angles greater than this maximum deflection angle, a single oblique shock cannot turn the free stream flow. While this condition still applies in the high Mach number regime, the fact that

https://doi.org/10.1017/S0022112097007131 Published online by Cambridge University Press

the flow downstream of the interaction point is underexpanded results in a more restrictive criterion for Type VI–Type V transition.

Unlike the Type VI–Type I transition line and the Type I–Type V transition line, the Type V–Type IV transition line must be calculated numerically. At low second wedge angles, this line approaches the maximum deflection angle for the inboard flow along the first wedge. The curved line labelled 'Bow shock detachment' represents the point at which the bow shock detaches from the nose of the wedge, while the lowest horizontal line labelled 'Oblique shock detachment' represents the point at which the nose shock is detached.

5. Conclusions

We have performed detailed simulations of steady inviscid shock interactions on double-wedge geometries. Four of the interactions that occur (Type VI, Type V, Type IV, and Type I) fit into Edney's classification scheme. One other interaction that we term a Type IVr also occurs. This new shock interaction is similar to a Type IV interaction, except that the shock which impinges on the wedge surface undergoes a regular reflection rather than a Mach reflection as in the Type IV interaction. The Type IVr interaction occurs because of the geometrical constraints of the double wedge and cannot occur for the type of blunt body flows investigated by Edney.

Our calculations show that there is a critical Mach number for these flows, above which the inboard flow along the wedge surface is always underexpanded with respect to the outboard flow. For Type V, Type IV, and Type IVr interactions this can result in an underexpanded supersonic jet along the surface. The interaction of this jet with the adjacent subsonic region results in large-amplitude steady pressure variations on the wedge surface. Below the critical Mach number, either underexpanded Type VI interactions or overexpanded Type I, Type V, or Type IV interactions occur. In the overexpanded interactions, the surface pressure decreases smoothly from a maximum at the corner of the wedges.

The transition criteria between the various interactions have also been identified. Below the critical Mach number, a Type VI–Type I transition occurs when the inboard and outboard flows downstream of the interaction region are perfectly expanded with respect to each other. A Type I–Type V transition occurs when the second wedge angle reaches the maximum deflection angle for the free-stream flow. Above the critical Mach number, a Type VI–Type V transition occurs when the outboard flow angle reaches the maximum deflection angle for the free stream. These transition criteria can be determined analytically using the method of characteristics, and the numerical results are in excellent agreement. The Type I–Type V and the Type VI–Type V transitions do not occur suddenly, but occur over a finite range of second wedge angles as the seven-shock Type V configuration develops. The Type V–Type IV and Type IV–Type IVr transition criteria cannot be predicted analytically and have been calculated numerically.

This work was supported by the Air Force Office of Scientific Research Grant Number F49620-93-1-0338 and NASA Langley Research Center Contract NAG-1-1498. This work is also sponsored in part by the Army High Performance Computing Research Center under the auspices of the Department of the Army, Army Research Laboratory cooperative agreement number DAAH04-95-2-0003 / contract number DAAH04-95-C-0008, the content of which does not necessarily reflect the position

https://doi.org/10.1017/S0022112097007131 Published online by Cambridge University Press

or the policy of the government, and no official endorsement should be inferred. Computer time was provided in part by the University of Minnesota Supercomputing Institute.

REFERENCES

Bertin, J. J. & Hinkle, J. C. 1975 Experimental investigation of supersonic flow past double wedge configurations *AIAA J.* **13**, 897–901.

Candler, G. V., Wright, M. J. & McDonald, J. D. 1994 Data-parallel lower-upper relaxation method for reacting flows. *AIAA J.* 32, **12**, 2380–2386.

Edney, B. 1968 Anomalous heat transfer and pressure distributions on blunt bodies at hypersonic speeds in the presence of an impinging shock. *Rep.* 115. Flygtekniska Forsoksanstalten (The Aeronautical Research Institute of Sweden), Stockholm.

Lamont, P. J. & Hunt, B. L. 1980 The impingement of underexpanded, axisymmetric jets on perpendicular and inclined plates *J Fluid Mech* **100**, 471–511.

MacCormack, R. W. & Candler, G. V. 1989 The solution of the Navier-Stokes equations using Gauss-Seidel line relaxation. *Computers Fluids* **17**, 135–150.

Olejniczak, J. & Candler, G. V. 1996 Study of experiments sensitive to vibration-dissociation coupling models. *Proc. 20th Intl Symp. on Shock Waves* (ed. B. Sturtevant, J. E. Shepherd & H. G. Hornung), pp. 323–328. World Scientific.

Olejniczak, J., Candler, G. V., Wright, M. J., Hornung, H. G. & Leyva, I. A. 1996 High enthalpy double-wedge experiments. *AIAA Paper* 96-2238.

Olejniczak, J., Wright, M. J. & Candler. G. V. 1996 Numerical study of shock interactions on double-wedge geometries. *AIAA Paper* 96-0041.

https://doi.org/10.1017/S0022112097007131 Published online by Cambridge University Press